TẠP CHÍ KHOA HỌC VÀ CÔNG NGHỆ ĐẠI HỌC DUY TÂN
DTU Journal of Science and Technology 02(75) (2026) 56-70
ĐẠI HỌC DUY TÂN
DUYTAN UNIVERSITY

Comparative Evaluation of Confinement Models for Reinforced Concrete Columns using Nonlinear Simulations in OpenSees

Đánh giá so sánh các mô hình kiềm chế nở ngang cho cột bê tông cốt thép bằng mô phỏng phi tuyến sử dụng OpenSees

Pham Phu Anh Huy[a,b*]
Phạm Phú Anh Huy[a,b*]

[a]*Institute of Research and Development, Duy Tan University, Da Nang, 550000, Viet Nam*
[a]*Viện Nghiên cứu và Phát triển Công nghệ cao, Đại học Duy Tân, Đà Nẵng, Việt Nam*
[b]*Faculty of Civil Engineering, School of Engineering and Technology, Duy Tan University, Da Nang, 550000, Viet Nam*
[b]*Khoa Xây dựng, Trường Công nghệ và Kỹ thuật, Đại học Duy Tân, Đà Nẵng, Việt Nam*

(Date of receiving article: 15/11/2025, date of completion of review: 29/01/2026, date of acceptance for posting:07/04/4026)

Abstract

This study presents a numerical evaluation of the axial behaviour of reinforced concrete (RC) columns confined with five widely used constitutive models (Mander et al., Attard & Setunge, Samani & Attard, Cusson & Paultre, and an unconfined reference) under eccentric compression and varying axial-load ratios. The results show that confinement effectiveness depends strongly on the degree of lateral dilation permitted by the axial load. At low axial-load ratios, confinement substantially improves peak strength, residual capacity, stiffness retention, and ductility due to the full activation of confining pressure. As axial compression increases, lateral dilation is progressively suppressed, limiting the mobilized confinement and causing the structural responses of all models to converge toward a common compression-controlled mechanism. At high axial-load ratios, confinement provides only marginal structural benefit, despite the large material-level strength and strain enhancements predicted by the constitutive laws. Stiffness degradation, ductility evolution, and post-peak softening all become insensitive to the choice of confinement model once axial compression dominates. These findings highlight the need to consider axial-load effects explicitly when selecting confinement models for nonlinear analysis and support the use of confinement-efficiency reduction approaches in performance-based seismic and robustness-oriented design.

Keywords: RC column, confinement model, axial load ratio, eccentric compression, ductility, stiffness

Tóm tắt

Bài báo trình bày một đánh giá bằng phương pháp số về ứng xử chịu lực dọc trục của cột bê tông cốt thép (BTCT) có xét đến hiệu ứng kiềm chế nở ngang (KCNN), sử dụng năm mô hình (Mander và cộng sự; Attard & Setunge; Samani & Attard; Cusson & Paultre; và trường hợp không xét KCNN), dưới tác dụng của nén lệch tâm và các tỷ số nén khác nhau. Kết quả cho thấy hiệu quả của cơ chế KCNN phụ thuộc chặt chẽ vào mức độ giãn nở ngang được cho phép bởi tải trọng dọc trục. Ở các tỷ số nén nhỏ, hiệu ứng KCNN làm tăng đáng kể cường độ cực đại, khả năng chịu lực dư, khả năng duy trì độ cứng và độ dẻo của cột, do áp lực KCNN được huy động đầy đủ. Khi lực nén dọc trục tăng, hiện tượng giãn nở ngang bị kìm hãm dần, làm hạn chế mức độ huy động của áp lực KCNN và khiến ứng xử kết cấu của các mô hình hội tụ

[*]*Corresponding author:* Pham Phu Anh Huy
Email: phampanhhuy@duytan.edu.vn

về một cơ chế làm việc chung do nén chi phối. Ở các tỷ số nén lớn, hiệu ứng KCNN chỉ mang lại lợi ích kết cấu hạn chế, mặc dù các mô hình vật liệu dự báo sự gia tăng đáng kể về cường độ và biến dạng ở cấp độ vật liệu. Sự suy giảm độ cứng, quá trình phát triển độ dẻo và hiện tượng mềm hóa sau đỉnh trở nên hầu như không còn nhạy cảm với việc lựa chọn mô hình KCNN khi lực nén dọc trục chiếm ưu thế. Những kết quả này nhấn mạnh sự cần thiết phải xét đến ảnh hưởng của tỷ số nén một cách tường minh khi lựa chọn mô hình KCNN trong phân tích phi tuyến, đồng thời ủng hộ việc áp dụng các cách tiếp cận giảm hiệu quả KCNN trong thiết kế theo hiệu năng kháng chấn và thiết kế hướng đến tính bền vững và an toàn kết cấu.

Từ khóa: cột bê tông cốt thép, mô hình kiềm chế nở ngang, tỷ số nén, nén lệch tâm, độ dẻo, độ cứng

1. Introduction

Reinforced concrete (RC) columns form the primary load-bearing components of most structural systems, transferring vertical and lateral loads from beams and slabs to the foundation. Their performance under combined axial compression and bending governs the global stability, ductility, and energy-dissipation capacity of the structure. In realistic loading conditions such as earthquakes, wind, or accidental eccentricities, columns seldom experience pure axial compression. Instead, they are subjected to a combination of axial load and bending moment [1–4]. One of the most decisive factors influencing the post-peak behaviour of RC columns is the confinement of concrete provided by transverse reinforcement. Confinement restrains the lateral expansion of the concrete core. It increases compressive strength and strain capacity, delays concrete crushing, and sustains load-carrying ability after the unconfined concrete reaches its peak stress. The seminal works by Mander et al. [5] and Park & Paulay [6] established the fundamental understanding of this mechanism. These studies demonstrated its critical importance in enhancing ductility and toughness, particularly for seismic-resistant members. The confining effect arises from the passive pressure induced by hoops or spirals acting in compression against the expanding concrete core. This interaction produces a triaxial stress state, which improves both the ultimate compressive strength f_{cc} and the corresponding strain ε_{cc}.

Over the past three decades, numerous analytical models have been proposed to describe the stress–strain behaviour of confined concrete. Among them, the model by Mander et al. [5] remains the most widely adopted. This is mainly due to its simplicity, rational derivation from equilibrium and compatibility principles, and applicability to both circular and rectangular sections. The Cusson & Paultre [7] model introduced improved expressions for confinement effectiveness in rectangular columns with closely spaced ties, accounting for the non-uniform confinement distribution. The Attard & Setunge [8] formulation refined the stress–strain relationship for high-strength concrete, while Samani & Attard [9] later extended it to cyclic loading conditions, providing continuous equations suitable for numerical implementation. Collectively, these models have become the foundation of nonlinear material modelling in advanced finite-element software such as OpenSees, ABAQUS, and DIANA.

Despite their widespread use, most confinement models were calibrated using axially loaded specimens. In such specimens, the stress state in the core concrete is largely uniform. Under eccentric compression, however, the stress distribution becomes highly non-uniform. One side of the section experiences compression, while the opposite side undergoes tension. As a result, the confining pressure is only partially activated. Experimental studies (e.g., Yu et al. [10]; Ni et al. [11]; Raafat and Khaled [12]) have shown

that, with increasing eccentricity, the effective confined zone diminishes and the overall ductility decreases. This reduction occurs even though the same amount of transverse reinforcement is present. This behaviour indicates that the effectiveness of confinement depends not only on geometric and material parameters but also on the applied axial load ratio and the resulting bending–compression interaction. The axial load ratio, defined as $n = P/(f_c' A_g)$, is a key nondimensional parameter governing column behaviour. A low value of n(typically $n \leq 0.1$) implies bending-dominant behaviour with high deformation capacity. In contrast, high axial-load ratios ($n \geq 0.6$) lead to compression-dominant behaviour and reduced ductility. Numerous experimental and numerical investigations have demonstrated that moderate axial loading ($0.1 < n < 0.7$) often provides an optimal balance between strength and ductility. In this range, the column benefits from both confinement effects and flexural deformation before instability occurs. However, when n exceeds approximately 0.6, crushing of the compression zone develops rapidly. Under such conditions, confining pressure cannot fully mobilize, and the load–deformation response becomes brittle [13–16].

Recent advancements in computational modelling and open-source platforms such as OpenSees [17] have made it possible to perform detailed nonlinear simulations incorporating both material and geometric nonlinearities. Geometric nonlinearity ($P - \Delta$ effect) becomes pronounced when large displacements occur, altering the internal-force distribution and either stabilising or destabilising the structural system depending on the boundary conditions. In the context of eccentric compression, this effect influences the evolution of curvature, secondary bending, and energy dissipation. By combining advanced confinement models with geometrically nonlinear analysis, the full progression of structural response can be captured. This progression includes elastic behaviour, yielding, post-peak softening, and eventual instability. Such an approach provides deeper insight into the true ductility capacity of the column.

Although several studies have explored the behaviour of confined concrete, a clear research gap remains. In particular, the response of different confinement models under varying axial-load ratios has not been sufficiently quantified within a unified computational framework. Existing comparisons have mainly focused on pure axial compression (e.g., Cusson & Paultre [18]; Samani & Attard [9]) or cyclic lateral loading of beam–column elements. Very few studies have systematically examined the interaction of confinement model choice and axial load ratio on both ductility and energy dissipation [19–21]. In the context of performance-based and robustness-oriented design frameworks, such energy-based measures are increasingly recognised as more reliable indicators of structural safety than strength-based parameters alone. For example, the total dissipated energy, E_d, during monotonic or cyclic loading corresponds to the area under the force–displacement curve. This quantity directly reflects the capacity of a column to absorb and redistribute energy during extreme events. Understanding how E_d varies with confinement model and axial load ratio provides essential guidance for developing simplified yet accurate analytical expressions suitable for design codes.

Another motivation for this study arises from the practical implementation of confinement models in finite-element analyses. In OpenSees, the Concrete02 material model requires a set of input parameters that differ slightly from those originally defined in each confinement model. Translating the parameters consistently across

models ensures that observed differences are due to the confinement theory itself rather than inconsistencies in implementation. This study therefore adopts a unified modelling framework where all confinement models are implemented through equivalent Concrete02 parameters, allowing fair and reproducible comparison.

Building upon this background, the present research conducts a comprehensive numerical evaluation of confinement models for RC columns subjected to combined axial compression and bending. Five widely used confinement models are considered: Unconfined, Mander et al., Attard & Setunge, Samani & Attard, and Cusson & Paultre. The analyses are performed for four representative axial-load ratios ($n = 0, 0.1, 0.4, 0.7$), covering the full transition from flexural-dominated to compression-dominated behaviour. A displacement-controlled framework with adaptive step size is employed to capture the complete nonlinear response, including strength degradation, stiffness loss, ductility development, and energy dissipation. The performance metrics extracted for each case include: (i) peak force and post-peak softening characteristics, (ii) normalized stiffness degradation, (iii) evolution of axial ductility, (iv) strength and strain enhancement indices, and (v) cumulative energy dissipation.

By comparing these responses across confinement models and axial-load ratios, the study aims to:

(1) quantify how confinement formulations influence strength, ductility, stiffness retention, and energy-based performance under varying axial compression;

(2) identify the axial-load ratio range within which confinement is most effective; and

(3) clarify the extent to which confinement efficiency diminishes, and model-to-model differences vanish, when axial compression becomes dominant.

The novelty of the present research lies in its systematic and unified evaluation of multiple confined-concrete constitutive models within a geometrically nonlinear simulation framework. Unlike previous studies that primarily focus on strength-based comparisons or isolated loading conditions, this study investigates confinement effectiveness across multiple structural performance dimensions under varying axial-load ratios. The key innovative contributions of this work are summarised as follows:

- A unified numerical framework is developed to implement multiple confinement models consistently within a geometrically nonlinear OpenSees environment, ensuring that observed differences arise from confinement theory rather than modelling inconsistencies.
- The interaction between confinement effectiveness and axial-load ratio is systematically quantified across the full transition from flexural-dominated to compression-dominated behaviour.
- Structural-level performance indicators (including peak strength, stiffness degradation, ductility evolution, post-peak softening, and cumulative energy dissipation) are jointly evaluated, rather than relying on strength alone.
- The divergence between material-level confinement enhancement and structural-level performance is explicitly demonstrated, highlighting how axial compression suppresses the mobilisation of confinement despite large constitutive strength and strain predictions.
- Axial-load ratio thresholds beyond which confinement effectiveness diminishes and model-to-model differences become negligible are identified, providing practical guidance for nonlinear analysis and design.

• Design-oriented implications are derived to support the calibration of nonlinear analysis tools and the development of simplified confinement-efficiency reduction factors applicable to seismic, robustness, and accidental-loading scenarios.

2. Methodology

2.1. Overview of confined models

To accurately capture the nonlinear stress–strain response of confined concrete under combined axial and flexural compression, several analytical formulations have been proposed over the past decades. Each model reflects a distinct theoretical foundation, experimental calibration, and confinement mechanism, ranging from classical equilibrium-based approaches to later empirical and energy-consistent formulations. While the general effect of confinement, enhancing strength, ductility, and energy absorption, is well established, the quantitative prediction of these enhancements varies considerably depending on the adopted constitutive model. Among the available models, four representative formulations have gained wide acceptance for both research and practical applications due to their simplicity, robustness, and compatibility with numerical tools such as OpenSees. The Mander et al. model [5], developed from the equilibrium of confining pressure and lateral expansion, provides a unified description for circular and rectangular sections and remains a benchmark in most design-oriented analyses. The Attard & Setunge model [22] extends this concept using a fractional polynomial expression to better represent high-strength concrete and to achieve smoother transition between the ascending and descending branches. Later, the Samani & Attard [9] formulation generalized this approach into a continuous unified equation valid for both monotonic and cyclic loading, ensuring numerical stability in nonlinear simulations. Finally, the Cusson & Paultre [18] model introduced confinement efficiency factors for rectangular columns with nonuniform tie spacing, incorporating fracture-energy concepts to represent post-peak softening and size effects.

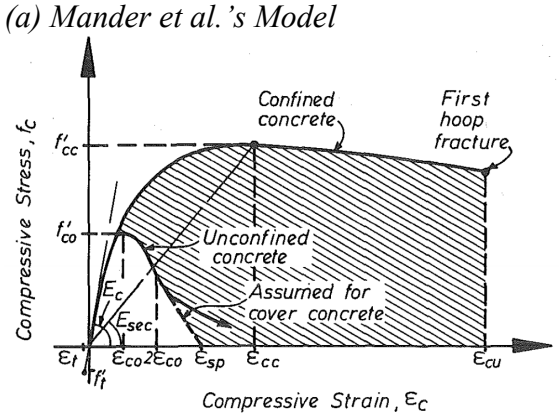

Figure 1. Mander et al. model [5]

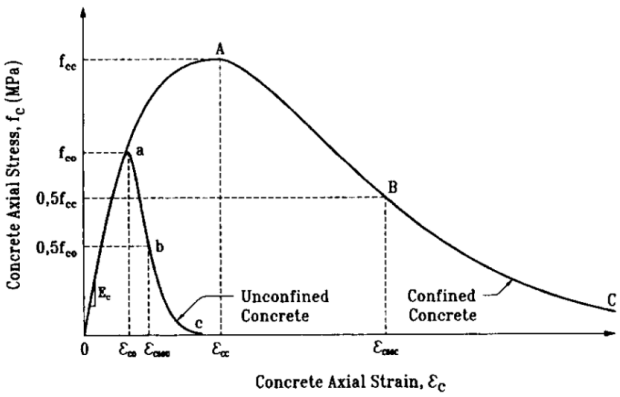

Figure 2. Cusson and Paultre model [18]

The confined-concrete model proposed by Mander et al. (as presented in Figure 1) is one of the most widely adopted formulations for RC members reinforced with transverse steel. The model modifies the unconfined stress–strain behaviour by incorporating the effective lateral confining pressure $f_{l,eff}$, which represents the average transverse pressure exerted on the concrete core. The enhancement in strength due to confinement is expressed as:

$$f'_{cc} = f'_{co}\left(2.254\sqrt{1+7.94\frac{f_{l,eff}}{f'_{co}}}-2\frac{f_{l,eff}}{f'_{co}}-1.254\right) \quad (1)$$

The corresponding strain at peak stress increases proportionally with the confinement level:

$$\varepsilon_{cc} = \varepsilon_{co}[\,1+5(\frac{f'_{cc}}{f'_c}-1)] \quad (2)$$

The ultimate strain, accounting for post-peak ductility, is given by:

$$\varepsilon_{cu} = \varepsilon_{cc}(1+0.2\frac{f_{l,eff}}{f'_c}) \quad (3)$$

where f'_c is the unconfined compressive strength of concrete: f'_{cc} is the peak compressive strength of confined concrete; f'_{co} is the unconfined concrete compressive strength; $f_{l,eff}$is the effective lateral confining pressure provided by transverse reinforcement; ε_{cc} is the strain corresponding to the confined peak stress f'_{cc}; ε_{co} is the strain at peak stress of unconfined concrete, typically around 0.002–0.003 for normal-strength concrete; $\varepsilon_{cu}$is the ultimate compressive strain of confined concrete, reflecting the improved post-peak deformation capacity resulting from confinement.

(b) Cusson and Paultre Model

The Cusson–Paultre model (Figure 2) represents an advanced confined-concrete formulation developed specifically for rectangular RC columns, accounting for nonuniform lateral restraint and fracture-energy considerations. The model introduces an improved confinement effectiveness coefficient that captures the actual distribution of lateral pressure within the concrete core and provides enhanced accuracy for both normal- and high-strength concrete.

The compressive strength of confined concrete increases linearly with the level of effective confinement:

$$f'_{cc} = f'_c(1+5.0\frac{f_{l,eff}}{f'_c}) \quad (4)$$

The corresponding peak strain is expressed as:

$$\varepsilon_{cc} = \varepsilon_{co}(1+7.5\frac{f_{l,eff}}{f'_c}) \quad (5)$$

The ultimate strain is enhanced significantly due to the model's fracture-energy-based softening formulation:

$$\varepsilon_{cu} = \varepsilon_{cc}(1+1.4\frac{f_{l,eff}}{f'_c}) \quad (6)$$

(c) Attard and Setunge Model

The Attard–Setunge model (Figure 4) provides a unified analytical stress–strain formulation for both confined and unconfined concrete across a wide strength range. The model ensures smooth continuity between the ascending and descending branches through a fractional polynomial expression and

incorporates the effects of confinement pressure through a small number of physically meaningful parameters.

The enhancement of compressive strength due to confinement is expressed as:

$$f'_{cc} = f'_c(1 + 4.1\frac{f_{l,eff}}{f'_c}) \tag{7}$$

The strain corresponding to the confined peak stress is estimated as:

$$\varepsilon_{cc} = \varepsilon_{co}(1 + 7.5\frac{f_{l,eff}}{f'_c}) \tag{8}$$

The ultimate strain, which controls the softening branch and overall ductility, is given by:

$$\varepsilon_{cu} = \varepsilon_{cc}(1 + 1.5\frac{f_{l,eff}}{f'_c}) \tag{9}$$

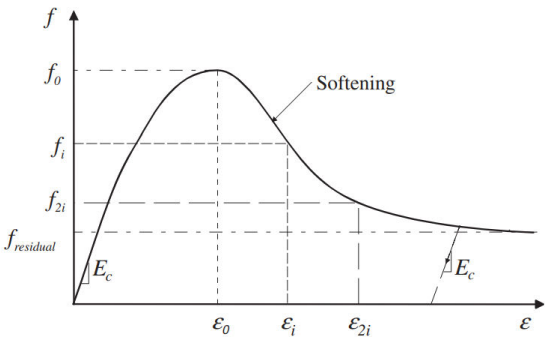

Figure 3. Attard and Setunge model [22]

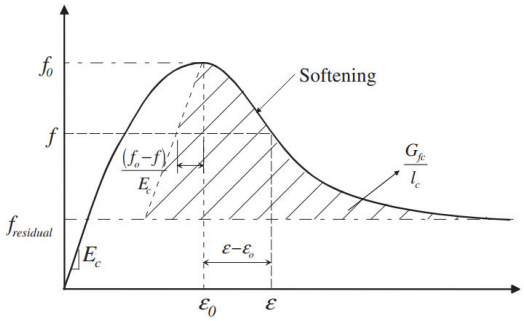

Figure 4. Samani and Attard model [9]

(d) Samani and Attard model

The Samani–Attard model provides a unified and continuous stress–strain formulation for both confined and unconfined concrete under monotonic or cyclic compression. Extending the Attard–Setunge model, it introduces a smooth fractional function that eliminates the need for piecewise definitions, making it numerically robust and well suited for nonlinear finite-element simulations.

The confined concrete strength increases linearly with the effective confining pressure:

$$f_{cc} = f_{co} + k_1 f_l \tag{10}$$

The corresponding peak strain is enhanced as:

$$\varepsilon_{cc} = \varepsilon_{co}(1 + k_2\frac{f_l}{f_{co}}) \tag{11}$$

The model provides an explicit confinement-dependent relation for the ultimate concrete strain:

$$\varepsilon_{cu} = \varepsilon_{co}(1 + k_3\frac{f_l}{f_{co}}) \tag{12}$$

where f_l is the nominal lateral confining pressure applied to the concrete core by the transverse reinforcement; k_1 is an empirical strength-enhancement coefficient that governs

the linear increase of confined compressive strength with respect to the applied lateral pressure f_l; k_2 is an empirical peak-strain enhancement coefficient, which controls the increase in the strain corresponding to peak stress; k_3 is an ultimate-strain enhancement coefficient, defining how much the ultimate strain grows as a function of lateral confinement.

3. Numerical modelling method

A numerical study was conducted to evaluate the axial response of a confined RC column subjected to eccentric compression under different axial-load ratios. All numerical analyses were performed using OpenSees version 3.7.1 (64-bit) [17], developed by the Pacific Earthquake Engineering Research (PEER) Center. The model represents a basic cantilever subassembly of a moment-resisting frame. The column height was $1.0m$ with a $300 \times 300mm$ square section, fixed at the base and loaded at the top with a constant eccentricity of $e/L = 0.1$. Four axial-load ratios, $n = \{0, 0.1, 0.4, 0.7\}$, were applied to represent bending-dominant to compression-dominant regimes. After preload application, vertical displacement was imposed to capture the complete response, including peak strength, post-peak softening, ductility, and energy dissipation.

Concrete was modelled using Concrete02, with five confinement laws (Unconfined, Mander et al., Attard & Setunge, Samani & Attard, Cusson & Paultre) incorporated through calibrated parameters $(f_c', \varepsilon_{c0}, f_{cu}, \varepsilon_{cu})$. Steel reinforcement followed Steel02 with Grade-400 properties. The column was represented by a nonlinearBeamColumn element in OpenSees with fiber-section discretisation (100 concrete fibers and four longitudinal bars). Five Gauss–Lobatto integration points were used along the element length, and geometric nonlinearity ($P-\Delta$) was included.

Analysis consisted of two stages: (1) gradual axial preload application using *LoadControl*, and (2) displacement-controlled eccentric compression using *DisplacementControl* with adaptive step reduction to ensure stable tracking into the softening range. Convergence was checked via *NormDispIncr* (tolerance 10^{-7}). At every step, axial force, lateral force, curvature, and top shortening were recorded. Cumulative energy dissipation was computed via the trapezoidal rule. This modelling strategy ensured robust evaluation of strength degradation, stiffness loss, ductility evolution, and residual capacity across all confinement models and axial-load ratios.

4. Results and discussion

The results presented and discussed in this section are obtained from nonlinear numerical simulations of the reinforced concrete column described in Section 3. All responses shown in Figures 5–8 are derived from the same geometrically nonlinear OpenSees model, incorporating different confined-concrete constitutive formulations and subjected to eccentric compression under varying axial-load ratios. The numerical results are analysed in terms of axial force–shortening behaviour, stiffness degradation, ductility evolution, and energy dissipation to enable a consistent and comparative assessment of confinement effectiveness.

4.1. Axial force–shortening and average stress–strain behaviour

The axial force–shortening and average stress–strain responses in Figure 5 can be interpreted directly from the mechanisms that govern lateral dilation, confinement activation, and compression–bending interaction. At zero axial load ($n = 0$), the compression zone experiences significant lateral expansion as soon as cracking initiates. This dilation activates the transverse reinforcement to its fullest capacity,

generating effective confining pressure that enhances both strength and deformation capacity. Consequently, the confined models exhibit peak force capacities that are 55–70% higher than those of the unconfined case (4200–5000 kN compared with approximately 3000 kN), and they develop an extended post-peak plateau sustained by stable confinement-induced resistance. The stress–strain curves show the same mechanism: lateral dilation continues to grow with increasing strain, allowing the confined core to reach 45–55 MPa, compared with only ~32 MPa for unconfined concrete, together with much larger ultimate strains. This behaviour reflects a fully flexural-dominated regime where confinement can mobilize steadily as the compression zone widens.

When a small axial load is applied ($n = 0.1$), the confinement mechanism remains effective but becomes less sensitive to the choice of confinement model. The axial load produces an initial compression that delays tensile cracking on the tension side and slightly restrains lateral dilation on the compression side. As a result, confined models still outperform the unconfined one markedly, but the spread among confinement formulations narrows. Physically, the early confining action is triggered more uniformly, leading to similar dilation patterns and similar peak-load and softening behaviours.

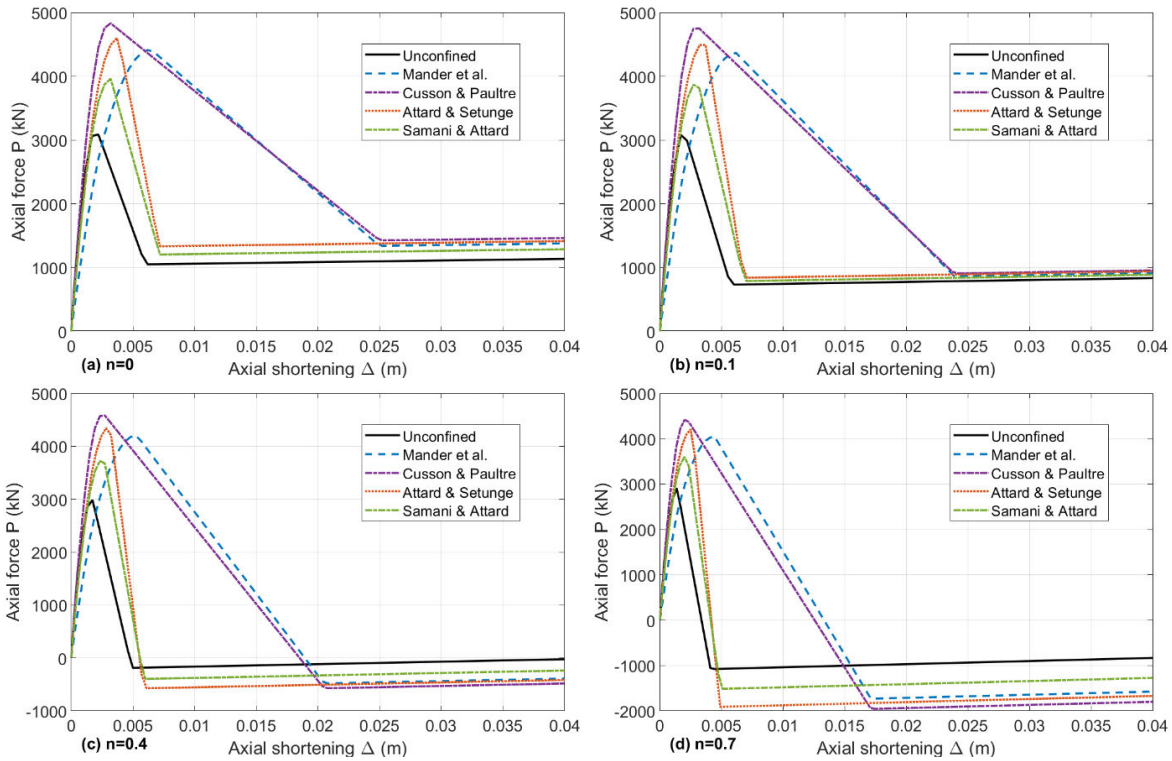

Figure 5. Axial force–shortening curves for different confinement models.

As the axial load increases to ($n = 0.4$), the stress field becomes compression-dominated. The high vertical compression suppresses lateral dilation, reducing the amount of confining pressure that can be mobilized during loading. This mechanism explains the noticeable reduction in strength enhancement and the steeper post-peak softening observed for all confined models. Because dilation is strongly restricted, confinement activation becomes incomplete, and the force–shortening curves of different confinement formulations begin to cluster. The column now behaves closer to an axially loaded strut, where strength is governed primarily by compression rather than confinement-induced tri-axiality.

At high axial load ($n = 0.7$), the confinement mechanism becomes largely ineffective. The compression zone crushes before significant dilation can occur, preventing the transverse reinforcement from developing meaningful confining pressure. This explains why all models, confined and unconfined, exhibit nearly identical peak strengths and brittle post-peak behaviour. The stress–strain curves converge sharply, showing negligible confinement-induced enhancement. Under this regime, the response is governed entirely by axial crushing and strain localization, reflecting a fully compression-controlled limit state.

Accordingly, these dilation-driven mechanisms explain why confinement provides substantial benefits only at low to moderate axial loads, while high axial compression forces all models to converge toward the same compression-controlled response.

4.2. Normalized stiffness degradation

The normalized stiffness trends in Figure 6 reveal a clear mechanistic relationship between axial-load ratio, lateral dilation, and confinement activation. At low axial load, the concrete core can dilate freely once cracking begins, enabling transverse reinforcement to develop confining pressure that delays stiffness degradation. As a result, confined models retain a substantially higher normalized stiffness: at strains of ε ≈ 3–4‰, they maintain $K_{sec}/K_0 \approx$ 0.30–0.45 whereas the unconfined column drops sharply to ≈0.20. This 50–120% improvement reflects the effective restraint of lateral expansion and delayed softening under low axial compression.

When the axial load increases to 0.4, the vertical compression suppresses lateral dilation, limiting the confining mechanism regardless of the confinement formulation. Consequently, the normalized stiffness of all confined models rapidly collapses into a narrow band of 0.10–0.15 by ε ≈ 3‰, with differences among models falling below 5%. The reduction of the confinement advantage at this axial level demonstrates that the stiffness response becomes governed primarily by axial compression, not by the specific confinement model.

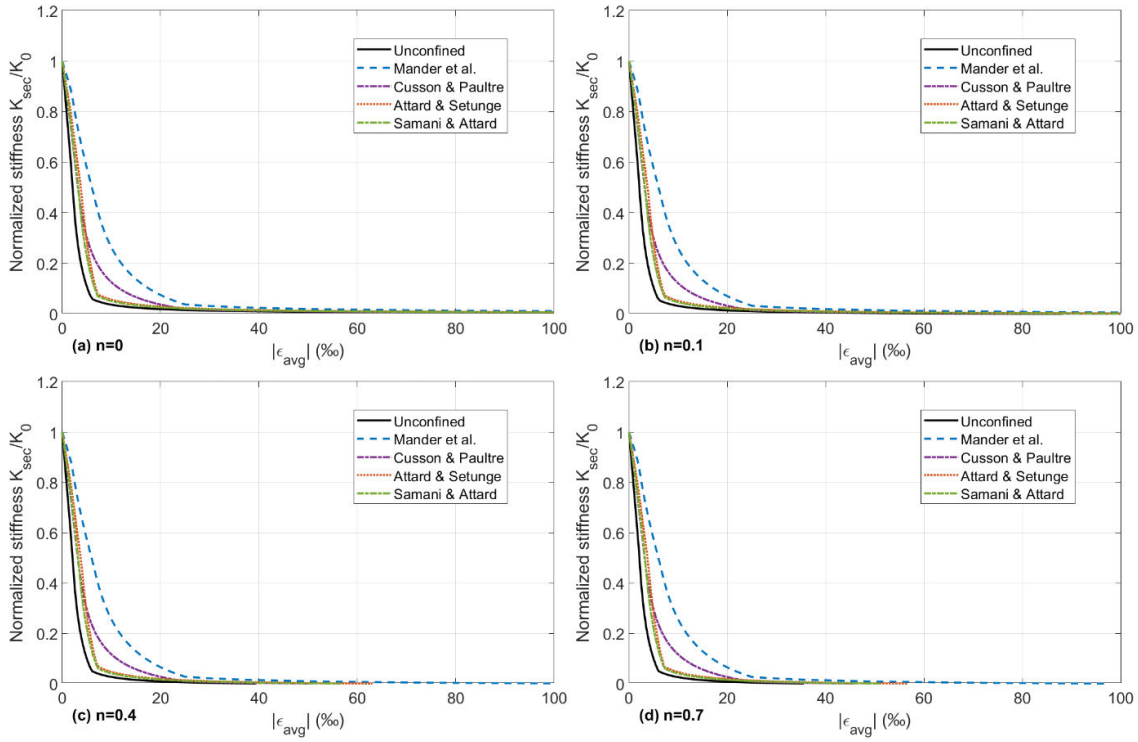

Figure 6. Normalized stiffness K_{sec}/K_0 versus axial strain.

At high axial compression ($n = 0.7$), dilation is inhibited almost entirely. Microcracking and crushing occur before meaningful confining pressure can develop, causing all curves, confined and unconfined, to drop below $K_{sec}/K_0 < 0.30$ within the earliest stages of shortening. Beyond ε ≈ 15–20‰, the normalized stiffness converges to a universal residual value of only 2–3% of the initial stiffness, indicating a fully compression-controlled mechanism where confinement provides negligible stiffness retention. The near-complete overlap of the curves at this stage confirms that the axial load ratio dominates the degradation process and suppresses any distinction among confinement formulations.

In summary, the normalized stiffness behavior demonstrates that confinement is effective only when lateral dilation is free to develop. As axial compression increases, dilation suppression prevents confining pressure from mobilizing, leading all stiffness trajectories to converge toward a common, rapidly degrading response that is largely insensitive to the chosen confinement model.

4.3. Evolution of axial ductility

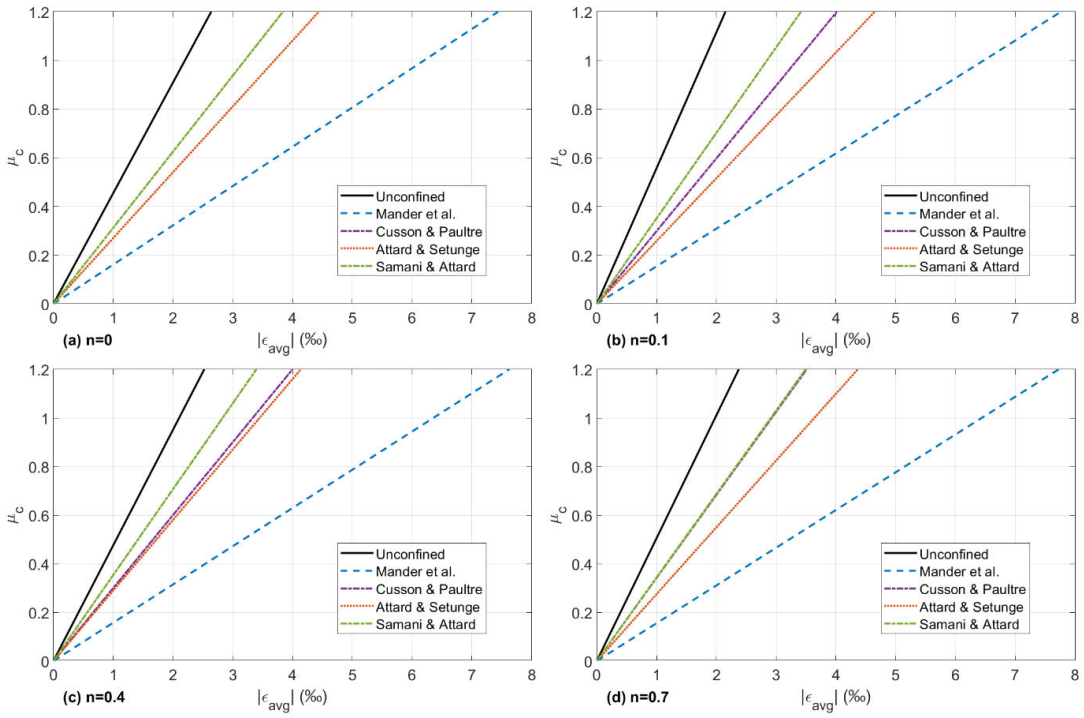

Figure 7. Evolution of axial ductility

The ductility evolution in Figure 7 can be understood by examining how axial compression alters the mechanisms of lateral dilation, neutral-axis depth, and strain localization in the compression zone. At zero axial load, the column behaves predominantly in a flexural-dominated manner, allowing the compression zone to dilate significantly as strain increases. This dilation enables the transverse reinforcement to mobilize confining pressure early and continuously, causing the confined concrete to sustain progressively larger strains before reaching the same ductility level as the unconfined concrete. Mechanically, the small neutral-axis depth and large curvature demand promote gradual stress redistribution, allowing confined models to reach 3–6‰ strain to attain, compared with only ≈2‰ for the unconfined case. This corresponds to a 70–200% increase in strain capacity, reflecting the full engagement of

the confinement mechanism under flexural-controlled behaviour.

Introducing a small axial load ($n = 0.1$) increases compression on the cross-section and raises the neutral-axis depth, which suppresses early dilation and reduces the tensile cracking on the opposite side. As a result, confinement is activated somewhat later, and the differences among the confined models shrink. Still, the dilation is sufficiently large for confinement to contribute meaningfully, and the ductility curves preserve the same ranking. The strains required to reach decrease slightly (typically 3.0–5.3‰), indicating that axial load begins to reduce (but not eliminate) the beneficial deformation capacity provided by confinement.

At moderate axial compression ($n = 0.4$), the behaviour transitions toward a mixed flexural–compression regime. The increased axial force produces a deeper compression block, limiting the width of the dilation zone and reducing the extent of tri-axial confinement stress that can develop. Consequently, confined models converge tightly, requiring only ≈3.0–3.4‰ strain to reach , with the Mander model maintaining slightly higher values due to its larger ultimate-strain prediction. This convergence is a direct outcome of reduced lateral dilation and earlier strain localization in the compression zone, which limit the ability of confinement to delay crushing.

At high axial load ($n = 0.7$), the response becomes fully compression-controlled. Lateral dilation is severely inhibited by the high vertical stress, preventing the confining ties from engaging effectively. Cracking and crushing in the compression zone occur rapidly, leaving little opportunity for confinement to influence the post-peak behaviour. Consequently, all confined models converge within a narrow strain range (2.8–4.2‰) to reach , and the unconfined curve essentially overlaps its low-n response. This tight clustering indicates that ductility is no longer governed by confinement characteristics but by axial-crushing mechanics and strain localization.

In general, the ductility response confirms that confinement is most effective only when axial compression is small, and its role diminishes rapidly as axial load forces the column into a crushing-controlled failure mechanism.

4.4. Strength and strain enhancement indices

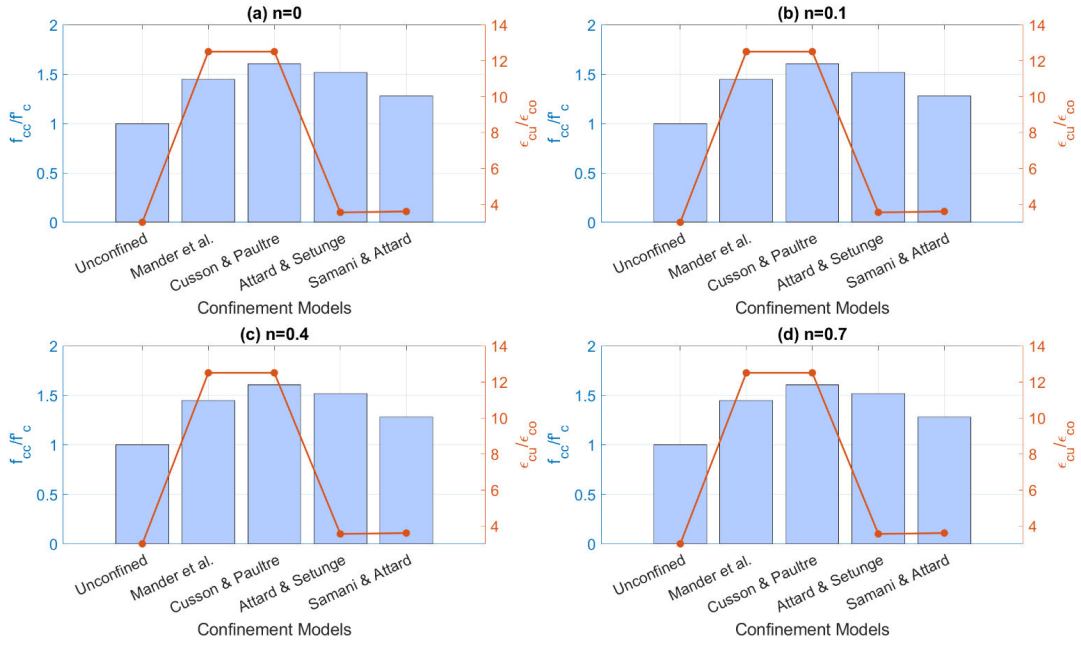

Figure 8. Strength and strain enhancement indices of confinement models.

The enhancement indices in Figure 8 provide a material-level perspective on confinement behaviour, revealing mechanisms that differ fundamentally from the structural responses observed in force–shortening, stiffness degradation, and ductility evolution. Across all axial-load ratios, the normalized strength enhancement and ultimate strain enhancement remain nearly constant for each confinement formulation. This invariance arises because these indices reflect intrinsic material properties, the degree to which each model predicts increased compressive strength and deformation capacity under full tri-axial confinement, rather than the actual degree of confinement realized at the structural level during loading.

At low axial load ($n = 0.1$), the structural response allows the concrete core to dilate sufficiently, enabling each confinement model to mobilize its predicted enhancement nearly to its full extent. Accordingly, the ranking among models is clearly expressed: strength enhancement ranges from 1.35 (Samani–Attard) to 1.70 (Cusson–Paultre), while ultimate strain enhancement spans from modest (~3 for Mander) to extreme (12–13 for Cusson–Paultre and Attard–Setunge). These differences stem from the constitutive formulations themselves, particularly the softening branch and the assumed confinement efficiency factors.

As axial load increases, the structural response becomes increasingly compression-dominated, which suppresses lateral dilation and reduces the confinement benefits that can actually be mobilized in the force–shortening, stiffness, and ductility responses. However, the enhancement indices in Figure 8 remain nearly unchanged. This is because these indices represent the potential material-level enhancement, specifically the predicted increases in confined strength and ultimate strain, and they do not depend on whether the structural conditions allow full confinement activation. Even when the axial-load ratio reaches 0.7 and the column behaves essentially as a compression-controlled strut, the constitutive models continue to provide the same enhancement factors because the input parameters that define the confined stress–strain envelope are not altered by the level of axial compression.

The persistence of these indices across n therefore reflects a fundamental mechanistic distinction: (1) Structural-level indicators (strength, ductility, stiffness) depend on mobilized confinement, which is strongly governed by lateral dilation and therefore highly sensitive to axial compression; (2) Material-level indices (strength & strain enhancement) reflect inherent confinement capacity, which is determined solely by the constitutive equations and remains stable regardless of the applied axial load.

This explains why strength enhancement remains in the 1.3–1.7 range across all n, and why ultimate strain enhancement remains dramatically different among confinement models, with Attard–Setunge and Cusson–Paultre consistently predicting order-of-magnitude increases relative to unconfined concrete. The structural-level convergence observed at high axial load does not alter the underlying constitutive definitions, hence the stability of the indices in Figure 8.

Overall, the trends confirm that enhancement indices capture theoretical confinement efficiency, while structural responses (force–shortening, stiffness, ductility) capture realized confinement performance. The discrepancy between these two perspectives widens as axial load increases and dilation becomes increasingly suppressed.

5. Conclusions

This study numerically evaluated five confinement models for RC columns under eccentric compression across four axial-load ratios. The results show that the effectiveness of confinement is strongly governed by the degree of lateral dilation permitted by the axial load. At low axial-load ratios ($n \leq 0.1$), confinement significantly enhances peak strength (by 55–70%), residual capacity, stiffness retention, and ductility, owing to the full mobilization of confining pressure. As the axial load increases to $0.1 < n < 0.7$, dilation is increasingly suppressed, reducing strength enhancement, accelerating stiffness degradation, and causing ductility curves to converge among confinement models. At high axial-load ratios ($n \geq 0.7$), the behaviour becomes compression-controlled and all models exhibit similar brittle responses, indicating that confinement plays only a minor structural role despite differences in their constitutive formulations. Material-level enhancement indices remain stable across , but the structural benefits diminish sharply once axial compression dominates. These findings highlight the need to limit axial-load ratios in columns expected to deform inelastically and suggest that advanced confinement models are most relevant at low axial loads, while simpler formulations may suffice when the response becomes model-insensitive at high compression.

Although comprehensive, the present study has several limitations. The simulations consider monotonic axial loading without cyclic or dynamic effects; bar buckling, bond slip, stirrup fracture, and construction imperfections were not explicitly modelled; and only one column geometry and reinforcement layout were investigated, which may limit the generality of the quantitative findings. Future research should therefore extend the analyses to cyclic and dynamic loading, incorporate bar buckling and bond-slip mechanisms, and investigate a broader range of sectional geometries and reinforcement details. Validation with large-scale experimental data and the development of data-driven or hybrid confinement models may further enhance predictive accuracy. Finally, integrating confinement effects into system-level analyses, including seismic performance and progressive-collapse scenarios, would support more robust structural design frameworks.

References

[1] Hany, N.F., Hantouche, E.G., Harajli, M.H. (2016). Finite element modeling of FRP-confined concrete using modified concrete damaged plasticity. *Engineering structures Journal* (125), 1–14. https://doi.org/10.1016/j.engstruct.2016.06.047.

[2] Ghani, M. U., Ahmad, N., Abraha, K.G., Manj, R.Z.A., Sharif, M.H., Wei, L. (2024). Review and assessment of material, method, and predictive modeling for fiber-reinforced polymer (FRP) partially confined concrete columns. *Polymers Journal* 16(10), 1367. https://doi.org/10.3390/polym16101367.

[3] Zeng, X. (2017). Finite element analysis of square rc columns confined by different configurations of transverse reinforcement. *The Open civil engineering Journal* (11), 292–302. https://doi.org/10.2174/1874149501711010292.

[4] KristombuBaduge, S., Mendis, P., Ngo, T.D., Sofi, M. (2019). Ductility design of reinforced very-high strength concrete columns (100–150 MPa) using curvature and energy-based ductility indices. *International Journal of Concrete structures and materials* (13), 1-23. https://doi.org/10.1186/s40069-019-0347-y.

[5] Mander, J.B., Priestley. M.J.N., Park, R. (1988). Theoretical stress-strain model for confined concrete. *Journal of Structural engineering* 114(8), 1804-1826. https://doi.org/10.1061/(ASCE)0733-9445(1988)114:8(1804).

[6] Park, R., Paulay, T. (1975). *Reinforced concrete structures*. USA:John Wiley & Sons, Inc. https://doi.org/10.1002/9780470172834.

[7] Cusson, D., Paultre, P. (1995). Stress-strain model for confined high-strength concrete. *Jouranl of Structural engineering* (121), 468–477. https://doi.org/10.1061/(ASCE)0733-9445(1995)121:3(468).

[8] Attard, M.M., Setunge, S. (1996). Stress-strain relationship of confined and unconfined concrete. *ACI Material Journal* 93(5), 432-442. https://doi.org/10.14359/9847.

[9] Samani, A.K., Attard, M.M. (2012). A stress–strain model for uniaxial and confined concrete under compression. *Engineering structures Journal* (41), 335-349. https://doi.org/10.1016/j.engstruct.2012.03.027.

[10] Yu, F., Zou, Q., Fang, Y., Wu, P., Huang, L., Bu, S. (2022). Experimental study on the eccentric performances of high predamaged rectangular reinforced concrete columns strengthened with carbon fiber reinforced polymer. *Structural concrete Journal* (23), 1735-1760. https://doi.org/10.1002/suco.202100195.

[11] Ni, X., Yuan, C., Li, Y. (2023). Experimental and analytical study on eccentric compressive behavior of concrete columns strengthened with high-strength reinforcement of HRB600. *Advances in Structural engineering Journal* 26(3), 428-447. https://doi.org/10.1177/13694332221125828.

[12] El-Hacha, R., Abdelrahman, K. (2020). Behaviour of circular SMA-confined reinforced concrete columns subjected to eccentric loading. *Engineering structures Journal* (215), 110443. https://doi.org/10.1016/j.engstruct.2020.110443.

[13] Saatcioglu, M., Razvi, S.R. (1992). Strength and ductility of confined concrete. *Jouranl of Structural engineering* 118(6), 1590-1607. https://doi.org/10.1061/(ASCE)0733-9445(1992)118:6(1590).

[14] Zhao, L., Cao, W., Guo, H., Zhao, Y., Song, Y., Yang, Z. (2018). Experimental and numerical analysis of large-scale circular concrete-filled steel tubular columns with various constructural measures under high axial load ratios. *Applied sciences Journal* 8(10), 1894. https://doi.org/10.3390/app8101894.

[15] El-Hacha, R., Abdelrahman, K. (2020). Behaviour of circular sma-confined reinforced concrete columns subjected to eccentric loading. *Engineering structure Journal* (215), 110443. https://doi.org/10.1016/j.engstruct.2020.110443.

[16] Kwan, A.K.H., Ho, J.C.M. (2019). Ductility design of high-strength concrete beams and columns. *Advances in Structural engineering Journal* 13(4), 651-664. https://doi.org/10.1260/1369-4332.13.4.651.

[17] Mazzoni, S., McKenna, F., Scott, M.H., Fenves, G.L. (2006). *OpenSees command language manual*. USA: University of California, Berkeley.

[18] Cusson, D., Paultre, P. (1995). Stress-strain model for confined high-strength concrete. *Journal of Structural engineering* 121(3), 468-477. https://doi.org/10.1061/(ASCE)0733-9445(1995)121:3(468).

[19] FallahPour, A., Gholampour, A., Zheng, J., Ozbakkaloglu, T. (2019). Behavior of FRP-confined high-strength concrete under eccentric compression: Tests on concrete-filled FRP tube columns. *Composite structures Journal* (220), 261-272. https://doi.org/10.1016/j.compstruct.2019.03.031.

[20] Isleem, H.F., Abid, M., Alaloul, W.S., Shah, M.K., Zeb, S., Musarat, M.A., Aslam, M.F., Alabduljabbar, H. (2021). Axial compressive strength models of eccentrically-loaded rectangular reinforced concrete columns confined with FRP. *Materials Journal*14(13), 3498. https://doi.org/10.3390/ma14133498.

[21] Lu, J.Y., Pang, W.W., Chang, S. (2013). Axial compression ratio limit of regional confined concrete columns. *Applied mechanics and Materials Journal* (438–439), 501-504. https://doi.org/10.4028/www.scientific.net/AMM.438-439.501.

[22] Attard, M.M., Setunge, S. (1996). Stress-strain relationship of confined and unconfined concrete. *ACI Materials Journal* 93(5), 432-442. https://doi.org/10.14359/9847.

[23] Popovics, S. (1973). A numerical approach to the complete stress-strain curve of concrete. *Cement and Concrete Research Journal* 3(5), 583–99. https://doi.org/10.1016/0008-8846(73)90096-3.